Dynamic Magnetic Resonance Imaging of Cerebral Blood Flow Using Arterial Spin Labeling

Afonso C. Silva and **Fernando F. Paiva**

Cerebral Microcirculation Unit, Laboratory of Functional and Molecular Imaging, National Institute of Neurological Disorders and Stroke, Bethesda, Maryland 20892 USA

Abstract

Modern functional neuroimaging techniques, including functional MRI, positron emission tomography and optical imaging of intrinsic signals, rely on a tight coupling between neural activity and cerebral blood flow (CBF) to visualize brain activity using CBF as a surrogate marker. Because the spatial and temporal resolution of neuroimaging modalities is ultimately determined by the spatial and temporal specificity of the underlying hemodynamic signals, characterization of the spatial and temporal profiles of the hemodynamic response to focal brain stimulation is of paramount importance for the correct interpretation and quantification of functional data. The ability to properly measure and quantify CBF with MRI is a major determinant of progress into our understanding of brain function. This chapter reviews the dynamic arterial spin labeling (DASL) method to measure CBF and the CBF functional response with high temporal resolution.

Keywords

functional magnetic resonance imaging; arterial spin labeling; animal models; cerebral blood flow; spatial resolution; temporal resolution

1. Introduction

A major goal of neuroscience and neurophysiology is to seek a deeper understanding of brain organization in terms of its anatomical and functional units (1). Modern neuroimaging methods, such as functional magnetic resonance imaging (fMRI) (2), positron emission tomography (PET) (3) and optical imaging of intrinsic signals (OIS) (4), are having an increasing role in mapping elemental functional units in the cerebral cortex. These functional imaging modalities rely on the coupling of cellular activity to the hemodynamic regulation of energy supply and waste removal – called "cerebrovascular coupling" – to detect the changes in cerebral blood flow (CBF), blood volume (CBV) or blood oxygenation, quantities that act as indirect surrogate markers of focal neuronal activity (5). Through the "cerebrovascular coupling", homeostasis of the brain parenchyma is maintained by regulation of CBF on a precise spatial and temporal domain (6–8). Because the spatial

Corresponding Author: Afonso C. Silva, Ph.D., Head, Cerebral Microcirculation Unit, Laboratory of Functional and Molecular Imaging, National Institute of Neurological Disorders and Stroke, National Institutes of Health, 10 Center Drive, MSC 1065, Building 10, Room B1D106, Bethesda, Maryland 20892-1065 USA, Phone: (301) 402-9703, Fax: (301) 480-2558, silvaa@ninds.nih.gov.

and temporal resolution of neuroimaging modalities is ultimately determined by the spatial and temporal specificity of the underlying hemodynamic signals, characterization of the spatial and temporal profiles of the hemodynamic response (HDR) to focal brain stimulation is of paramount importance for the correct interpretation and quantification of functional data (5) and significant effort has been placed on understanding the nature of the cerebrovascular coupling (9,10).

In the spatial domain, the CBF response to neural activity is well localized within the active cortex. In rat primary somatosensory cortex (S1), for example, elemental vascular units supply individual whisker barrels (11–13). The units are functionally linked for precise focal regulation of CBF, with the highest resting values and the highest changes being localized in layer IV (14). The physiological basis of the differences in CBF increments between different layers may be pericytes placed strategically to regulate capillary blood flow to meet local demands (15,16), or differences in capillary density accompanying differences in synaptic function (12,17,18). The match between microvascular structures and neural columns (13) ensures the CBF response is spatially specific to the activated column (19). Indeed, since the mid 1990's, several fMRI and OIS studies successfully mapped elemental functional units in the cortex, such as individual whisker barrels in rat S1 (20–22), individual digits in human sensorimotor cortex (23,24), cortical laminae in olfactory bulb (25,26) and S1 (27–29) of rodents, and ocular dominance or orientation columns in the cat and human visual cortex (19,30–39).

In the temporal domain, the HDR consists of several processes with different time scales. Through cerebrovascular coupling, local decreases in vascular resistance lead to an increase in local blood volume and flow. The increase in blood flow results in hyperoxygenation of the capillary bed that drains into the veins, causing a signal that forms the basis of BOLD contrast (2). The increased hyperoxygenation becomes prominent in medium to large draining veins, and thus this response is often considered to be spatially nonspecific. Upon cessation of the increased electrical activity, the neurovascular coupling causes restoration of the capillary and arteriolar volume, resulting in restoration of local CBF and of the imaging signal, once the transit of oxyhemoglobin across the local cerebral vasculature is completed (40). Thus, the temporal resolution of neuroimaging techniques is limited by vascular transit times. Recently, much effort has been placed on determining the "hemodynamic impulse response" (HIR) function as a way to understand the minimal evolution of vascular events and so that responses to complex neural activity can be modeled and predicted (40–45). For example, in rats, the OIS response to a 2-s-long whisker or forepaw stimulus begins 0.5–1 s after stimulus onset, peaks at 2.5–3 s, and returns to baseline by 4–5 s (40,42–46). In humans, the full-width-at-half-maximum (FWHM) is 5–7 s (47–49), and can be improved to 3–4 s if the contribution from large vessels is removed (50).

There is a growing body of evidence indicating that the fundamental spatial and temporal characteristics of the HDR are fine enough to resolve subcortical activity and suggesting that hemodynamic regulation occurs at a spatial scale that is much finer than the resolution of typical current human or animal fMRI, and implies that higher information content can be obtained with further technological improvements. However, it is not clear to what extent

hemodynamic signals will be able to map elemental neuronal populations, and thus continued research on understanding the spatial and temporal evolution of the HDR will be essential to increase the applicability of neuroimaging to the study of functional brain organization. The ability to properly measure and quantify CBF with MRI is a major determinant of progress into our understanding of brain function. This chapter reviews the dynamic arterial spin labeling (DASL) method to measure CBF and the CBF HDR with high temporal resolution.

2. Dynamic Arterial Spin Labeling

Cerebral blood flow can be measured with MRI by using endogenous arterial water as a perfusion tracer according to a number of approaches collectively known as arterial spin labeling (ASL) (51–54). The major advantages of ASL are that non-invasive and quantitative measurements of CBF can be performed and repeated indefinitely. Unlike other MRI methods for measuring CBF that use exogenous contrast agents, in ASL the tracer is imaged against the brain tissue water background. Therefore, the general principle of ASL is to differentiate the net magnetization of arterial water flowing proximally to the brain from the net magnetization of brain tissue water. The labeled arterial water flows through the brain, causing a net decrease in magnetization due to its mixing (with or without exchange) with the brain tissue water, which is proportional to the flow rate and therefore it may be used to calculate CBF in the conventional units of $\left[\frac{ml\ blood}{100\ g\ tissue \cdot min}\right]$. In addition, it is necessary to acquire two images, usually in an interleaved manner, to determine CBF: one with spin labeling, and another as a control. Thus, the ASL methods suffer from poor temporal resolution, which is typically on the order of a few seconds.

The formalism for ASL closely follows the one developed by Kety for monitoring the kinetics of freely diffusible tracers (55,56). In ASL, the brain tissue longitudinal magnetization can be described by the Bloch equations, modified to include the effects of CBF:

$$\frac{dM_b(t)}{dt} = \frac{M_b^0 - M_b(t)}{T_{1b}} + CBF \cdot \left[M_a(t) - M_v(t) \right] \quad [1]$$

where M_b is the brain tissue magnetization per gram of tissue, M_b^0 is the equilibrium value of M_b, T_{1b} is the longitudinal brain tissue relaxation time constant, CBF is the cerebral blood flow expressed in units of $\left[\frac{ml\ blood}{g\ tissue \cdot s}\right]$, and M_a and M_v are the arterial and venous blood magnetization per ml of blood, respectively. The above equation describes brain tissue as a single-compartment that is constantly receiving blood from the arterial side and losing blood water on the venous side. Assuming water to be a freely-diffusible tracer, the venous magnetization equals the brain magnetization according to:

$$M_v(t) = \frac{M_b(t)}{\lambda} \quad [2]$$

where λ is the brain-blood water partition coefficient, defined as the ratio of the amount of water per gram of tissue and the amount of water per ml of blood. In equilibrium, the amount of water delivered by the arterial vasculature to the tissue compartment must equal the amount of water leaving that compartment on the venous side:

$$M_a^0 = M_v^0 = \frac{M_b^0}{\lambda} \quad [3]$$

Therefore, Eq. [1] can be rewritten as:

$$\frac{dM_b(t)}{dt} = \frac{M_b^0 - M_b(t)}{T_{1app}} - 2 \cdot \alpha(t) \frac{CBF}{\lambda} M_b^0 \quad [4]$$

with the apparent longitudinal relaxation time for tissue water in the presence of perfusion, T_{1app}, and the degree of labeling efficiency, $\alpha(t)$, defined as:

$$\frac{1}{T_{1app}} = \frac{1}{T_{1b}} + \frac{CBF}{\lambda}$$
$$\alpha(t) = \frac{M_a^0 - M_a(t)}{2M_a^0} \quad [5]$$

Equation [4] tells us a number of important things about ASL. First, to cause a change in brain tissue magnetization related to perfusion, one needs to label blood (i.e., $\alpha(t)$ must be different than zero). Second, the perfusion rate does not instantly change brain tissue magnetization, but it does so with a time constant given by T_{1app}. Third, because CBF is only on the order of 60 ml blood/100 g tissue-minute, $CBF/\lambda \approx 0.01$ s^{-1}, the impact of CBF on T_{1app} is much too small to allow CBF to be reliably measured from changes in relaxation rates. Traditionally, ASL techniques have been presented as belonging to one of two basic implementation categories (52,57). In the first approach, arterial water is continuously labeled proximally to the region of interest in the brain (58,59). This approach is referred to as continuous ASL (CASL). In the second approach, a single, yet large volume of arterial blood is dynamically labeled proximally to the region of interest and allowed to flow into the tissue prior to data collection (60–63). This approach is generally referred to as pulsed ASL (PASL). A detailed comparison of CASL and PASL techniques can be found in (64), and is beyond the scope of this chapter.

The CASL approach is attractive for providing better sensitivity than PASL. In CASL, arterial water is continuously saturated ($\alpha_0 = \alpha(0) \approx 0.5$) or inverted ($\alpha_0 \approx 1.0$) proximally to the brain for a period long enough to allow the establishment of a steady-state in brain tissue magnetization. For a constant degree of labeling efficiency $\alpha(t) = \alpha_0 e^{-\tau/T_{1a}}$, where α_0 is the labeling efficiency at the labeling site, τ is the transit-time from the labeling site to the detection site, and T_{1a} is the longitudinal relaxation of arterial water, a steady-state $M_b^{label} = M_b(t)\big|_{t>5T_{1app}}$ is reached in which:

$$\Delta M = M_b^0 - M_b^{label} = 2\alpha T_{1app} M_b^0 \frac{CBF}{\lambda} \quad [6]$$

Thus, the CBF can be obtained from two images obtained with ($\alpha \neq 0$) and without ($\alpha = 0$) labeling:

$$CBF = \frac{\lambda}{2\alpha T_{1app}} \cdot \frac{M_b^0 - M_b^{label}}{M_b^0} \quad [7]$$

Equation [7] shows that CBF depends on the partition coefficient λ and on three additional parameters: the longitudinal tissue relaxation time T_{1b}, the transit time τ from the site of labeling to the site of interest in the tissue, and the difference in tissue MR signal between the control and the labeled states of magnetization. Commonly, these parameters are obtained in separate experiments. Furthermore, the parameters are measured usually in single instances, precluding dynamic analysis of fast variations. In many applications, as for example in functional MRI experiments aimed at determining the HDR with high temporal resolution, or in measurement of vascular transit-time maps associated with diagnosis of cerebrovascular diseases, it would be essential to determine CBF dynamically. One efficient way to accomplish dynamic measurements of CBF with ASL is to impose a systematic and periodic variation of the degree of labeling $a(t)$. According to Eq. [4], periodic variations in $a(t)$ would cause periodic variations in the tissue magnetization, and a temporal analysis of the tissue response would yield dynamic quantification of T_{1b}, τ and CBF. This transient analysis has been named dynamic ASL (DASL) (53,65).

The dynamic analysis can be introduced by simply allowing the degree of labeling $a(t)$ in Eq. [5] to be a time-dependent, periodic function. In such case, Eq. [4] can be integrated characterizing the time evolution after steady-state has been reached of a system subject to a specific time-varying labeling function, and is given by (65):

$$M_b(t) = M_b^0 - 2\alpha(t) M_b^0 \frac{CBF}{\lambda} e^{-\tau/T_{1a}} \otimes e^{-(t-\tau)/T_{1app}} \quad [8]$$

where $\otimes$ denotes the convolution product. From Eq. [8], it is important to notice that independently of the labeling function, the tissue response has a time shift introduced by the transit time τ.

In theory, the labeling function may be arbitrarily defined as long as the arterial spins can be inverted accordingly, so that definition of the labeling function should be determined by the experimental goals. For example, the use of a periodic square labeling function of period 2 defined as follows:

$$\alpha(t) = \begin{cases} \alpha_0 \cdot e^{-\tau/T_{1a}} & , \quad 0 < t \le \Delta \\ 0 & , \quad 0 < t \le 2\Delta \end{cases} \quad [9]$$

will produce a periodic tissue magnetization response, given by (65):

$$M_b(\tau < t \le \Delta + \tau) = M_b^0\left[1 - 2T_{1app}\alpha_0 e^{-\tau/T_{1a}}\frac{CBF}{\lambda} \times \left(\frac{\left(1 - e^{-\Delta/T_{1app}}\right)e^{-(t-\tau)/T_{1app}}}{e^{\Delta/T_{1app}} - e^{-\Delta/T_{1app}}} + \left(e^{-(t-\tau)/T_{1app}}\right)\right)\right]$$

$$M_b(\Delta + \tau < t \le 2\Delta + \tau) = M_b^0\left[1 - 2T_{1app}\alpha_0 e^{-\tau/T_{1a}}\frac{CBF}{\lambda} \times \left(\left(\frac{\left(1 - e^{-\Delta/T_{1app}}\right)e^{-\Delta/T_{1app}}}{e^{\Delta/T_{1app}} - e^{-\Delta/T_{1app}}} + \left(1 - e^{\Delta/T_{1app}}\right)\right)e^{-(t-\Delta-\tau)/T_{1app}}\right)\right] \qquad [10]$$

Figure 1 shows the tissue response expressed by Eq. [10] simulated for different frequencies of a square labeling function. As expected, the tissue response is shifted with respect to the labeling function by the transit time τ. Also, both amplitude and the phase of the tissue response are modulated by the labeling function. The phase modulation occurs due to the way the labeling function alters the magnetization of the arterial water flowing to the detection site, while the amplitude modulation occurs due to how fast the labeled and unlabeled states are switched when compared to the transit time and to the longitudinal relaxation rate. The DASL technique has the advantages of allowing continuous repetition of the ASL experiment in such a way that the tissue response can be analyzed to unravel in a dynamic manner the three parameters of interest: T_{1b}, τ and CBF. Determination of these parameters can be accomplished with high sensitivity, because the labeling period 2 can be made long enough so that the tissue response reaches steady-state (e.g., Fig. 1c) and because the periodic nature of the response facilitates analysis of the data in the frequency domain, allowing for frequency filtering of noise and other components with frequencies outside the model. It is important to notice that even though higher frequencies increase the number of cycles acquired in a given amount of time, thus improving the averaging process, their use may compromise the ability of accurately estimate T_{1app}, due to a decrease in the time span of evolution of the tissue magnetization and a decrease in the number of data points used for estimation of this parameter. On the other hand, the precision of estimation of the transit time τ is proportional to how accurately the temporal shift between the labeling function and the tissue response can be measured, and for this a higher sampling rate is required. For accurate transit time estimation, the sampling rate of the DASL curve must be higher than the smallest expected transit time. This can be a significant limitation in studies of small animals where the transit times can be quite short, on the order of 100 – 350 ms (53,65,66).

The DASL sampling scheme is particularly advantageous in the presence of periodic noise and other sources of signal fluctuation, such as the ones introduced by respiratory and cardiac cycles. In such cases, the periodic nature of the tissue response to a periodic labeling function greatly facilitates filtering of such noise sources. Efficient filtering can be accomplished by fitting the raw data to the model described by Eq. [10]. A simple Fourier transform (FT) of the model determines the allowed spectrum of frequencies, while the FT of the data reveals the periodic perturbations present in the data. A complex filter comprised of real and imaginary components present in the allowed spectrum of frequencies can be applied to the dataset to eliminate every frequency other than the ones predicted by the model.

Figure 2 illustrates the filtering process based on the DASL model for data obtained from an isoflurane-anesthetized rat at 7T. The original DASL time course is shown in Fig. 2a. A labeling frequency of 0.05Hz was used to generate the DASL time-course. The labeling time *TL* was 200 ms and the image repetition time *TR* was 250 ms. In spite of the good SNR,

noise present in the data is quite visible. Fig. 2b shows the real and imaginary components of the FT of the data, while Fig. 2c shows the frequency components allowed by the best fit of the data to the model in Eq. [10]. Fig. 2c shows the filtered data based on the frequencies allowed by the model. Negative amplitudes were removed by the filter, as well as the frequency component around 1Hz corresponding to the respiratory rate. The filtered DASL time course is shown in Fig. 2e, demonstrating the effectiveness of the filter in removing the noise and other unwanted fluctuations. The advantage of this filtering approach is that even perturbations occurring at very low frequencies can be taken out of the data without compromising the tissue response information. In theory, this should also enable to eliminate the contributions of large vessels to the CBF map. Assuming that the arterial protons flowing through the large vessels are flowing fast enough and do not exchange with tissue, they should not behave as predicted by the model in such a way that their contribution would be filtered out of the dataset and, thus, not considered in the final fitting that would be used to generate a CBF map. After filtering, the CBF, T_{1b} and transit time maps were obtained from the data and are shown in Figure 3a–c, respectively. The average whole-brain CBF value was 149 ml/(100g ·min) (Fig. 3a). Note the high SNR of the CBF map. The transit-time map, shown in Fig. 3c, had an average value of 258 ms, which is in excellent agreement with previously published values for the transit-time in rats (53,65,66).

3. Applications of DASL to Measurement of the Hemodynamic Response to Functional Brain Stimulation

As mentioned above, the temporal resolution of ASL methods for quantifying CBF is inherently low, due to the need of acquisition of two distinct images and because proper perfusion contrast is achieved only when enough time is allowed for the labeled spins to travel into the region of interest and exchange with tissue spins. The DASL technique is attractive in improving the temporal resolution of ASL, because data can be acquired with a high sampling rate while the magnetization state of the brain oscillates between the control and the steady-state conditions induced by the periodic labeling function.

In order to obtain high temporal resolution, short ASL RF pulses are used interleaved to an ultra-fast imaging sequence, such as echo-planar or spiral imaging (67). A compromise must exist between using ASL RF pulses that are short enough to allow for high temporal resolution, but long compared to the imaging time so that high labeling duty-cycles (and thus labeling efficiency) can be maintained. Specifically, between the acquisition of two consecutive images with a short repetition time (*TR*), ASL is achieved by a labeling RF pulse of length *TL*. According to this scheme, labeling of the arterial spins can be done with a duty-cycle $k = TL/TR$. If *TL* is not too short compared to *TR*, the duty-cycle k is high enough to preserve the sensitivity of the CASL technique. The proper determination of quantitative CBF maps requires a correct measure of the degree of arterial spin labeling, $\alpha(t)$. The new definition of $\alpha(t)$ to account for the labeling duty-cycle k is given by:

$$\alpha(t) = \begin{cases} k \cdot \alpha_0 \cdot e^{-\tau/T_{1a}} & , \quad 0 \le t \le \Delta \\ 0 & , \quad 0 \le t \le 2\Delta \end{cases} \quad [11]$$

Eq. [11] shows that the effect of using the DASL scheme as described above is to decrease the efficiency of labeling by the duty-cycle factor k. For example, ASL RF pulses of 78 ms duration were implemented in conjunction with a 30 ms readout EPI sequence (27,67). Under these conditions, CBF images could be formed every 108 ms, however, with a decreased labeling efficiency due to the lower duty-cycle $k = 0.72$. Similar DASL data, acquired using $TL = 200$ ms and $TR = 250$ ms, are shown in Figure 4. In this case, $k = 0.8$.

To demonstrate the usefulness of DASL in probing the CBF response to functional brain activation, DASL experiments were performed during bilateral somatosensory stimulation in an α-chloralose anesthetized rats at 7T. A labeling frequency of 0.0167 Hz was used corresponding to a half-period ═ 30 s. The functional paradigm was defined so that 3 s-long stimulus were presented during the stationary period of the DASL cycles. The stimulus parameters were: current amplitude = 2 mA, pulse width = 333 μs and repetition rate 3Hz. Fig. 4a shows a t-score map of the BOLD functional response. Robust activation regions were present in both left and right primary somatosensory cortices. Fig. 4b shows the combined DASL-fMRI time-course. The functional hemodynamic response can be easily noticed on top of the DASL experiment. The control phase of the DASL cycle displays a robust BOLD response, while the labeling phase shows the mixing of the functional BOLD and CBF contrast in anti-phase to each other. Because functional increases in CBF lead to signal decreases in ASL, the resulting functional signal changes are smaller during the labeling half-cycles (when the BOLD contrast opposes the CBF contrast) than during the control half-cycles (when contrast is due to BOLD alone). After fitting and filtering of the DASL curve, the data was averaged into a single DASL cycle, shown in Fig. 4c. The hemodynamic response is superimposed on the DASL evolution. Stimulation periods are indicated by the horizontal bars underneath the hemodynamic response.

Once the CBF images are formed, analysis of the temporal characteristics of the CBF response to functional stimulation is desired. For this, a temporal deconvolution of the measured MRI time-course becomes necessary, because instantaneous changes in CBF cannot be quickly reflected in the MRI time-course. To show this, consider the longitudinal tissue magnetization obtained after n RF pulses is (68):

$$M_z(n \times TR) = \frac{M_0 \left(1 - e^{-TR/T_{1\,app}}\right)}{1 - \cos\theta \cdot e^{-TR/T_{1\,app}}} + \frac{M_0 \left(1 - \cos\theta\right) e^{-TR/T_{1\,app}}}{1 - \cos\theta \cdot e^{-TR/T_{1\,app}}} \cdot \cos^n\theta \cdot e^{-nTR/T_{1\,app}} \quad [12]$$

The first term in Eq. [12] represents the longitudinal magnetization at the steady state condition, and the second term represents its dynamic evolution from the fully relaxed condition to the steady state condition. The basic principle of the ASL technique is the transfer of the longitudinal magnetization state of the endogenous labeled arterial water to the perfused tissue. According to Eq. [12], this transfer is limited by T_{1app}, by TR, and by the excitation RF flip angle θ. Thus, it cannot occur instantly. As a consequence, quick changes in CBF such as the ones produced by focal brain stimulation are only reflected a few seconds later in the tissue magnetization, and thus the MRI time-course measured in response to a quick change in perfusion is delayed. However, the transfer function that governs the delayed MRI response to step changes in CBF (and in T_{1app}) is inherently

present in Eq. [12] in the form of the signal evolution from the equilibrium magnetization state M_0 to the new steady-state magnetization expressed by the first term in Eq. [12]. Provided that it is measured during the MRI measurements of the functional CBF response, the transfer function can be used as a deconvolution kernel to remove the latency in the CBF response imposed by the MRI signal evolution. After the deconvolution process, the resulting CBF time-course reflects accurately the dynamics of the actual CBF changes.

Using an acquisition scheme that consisted of employing short ASL RF pulses in conjunction with an ultra-fast imaging sequence, we were able to measure the CBF response to somatosensory stimulation in α-chloralose anesthetized rats with a temporal resolution of 108 ms (27,67). Figure 5a shows the MRI-estimated CBF time-course (gray), and the deconvolved CBF time-course (black), in response to a 20 s-long stimulus. To obtain the true temporal dynamics of the CBF response, the MRI-estimated CBF curve was deconvolved with the initial ten seconds of the control magnetization decay, generating the deconvolved CBF signal. It can be clearly seen how the CBF response measured with MRI is delayed with respect to the deconvolved curve. One drawback of the deconvolution process is that it adds oscillatory noise to the data. However, the CBF changes elicited by somatosensory stimulation in α-chloralose anesthetized rats are quite robust and immune to the small amount of noise introduced by deconvolution of the original functional ASL curve. One important advantage of the use of DASL acquisition strategies in functional MRI is that the control cycle of the ASL curve can be used to obtain the BOLD functional changes so that this more popular fMRI contrast mechanism can be directly compared to the corresponding CBF changes.

Figure 5b shows the onset time of BOLD and CBF in the superficial and deep regions of the somatosensory cortex following the onset of stimulation. The onset of CBF changes in the deep layers of the somatosensory cortex occurred earlier than the corresponding BOLD changes (P < 0.003) (27). However, in the superficial layers, the onset of the CBF response was delayed and it was similar to the latency of the superficial BOLD signal changes. Figure 5C shows the BOLD and CBF times-to-peak. The CBF peak response occurred faster than the BOLD response in both regions (P < 0.001) (27). The heterogeneity of fMRI onset-times across the cortical depth layers is indicative of the effects of the vasculature on the fundamental temporal characteristics of the HDR, and make a clear statement that the resolution of fMRI is fine enough to resolve subcortical activity and to study subcortical processes, such as columnar and laminar cortical communication.

Indeed, the shorter onset times found with CBF in the deeper layers of the cortex (27) were later confirmed with BOLD contrast obtained at higher spatial resolution (28) (Table 1). The BOLD onset times obtained at high spatial resolution ($200 \times 200 \ \mu m^2$) from layers IV–V in the cortex (28) were as fast as the CBF onset-times obtained at a lower spatial resolution (27,67), suggesting that the onset-time of the hemodynamic response is faster than 600 ms and that improving the spatial resolution may further shorten the onset latency. In the latter study, layer-specific heterogeneity was maintained throughout the entire rising portion of the BOLD HDR, both in amplitude as well as in temporal aspect. Our data showed that layers IV–V in the rat somatosensory cortex have the strongest temporal resemblance to the stimulation paradigm, and that the onset times from those cortical laminae are shorter than

the respective latencies from layers I–III and VI, suggesting that the HDR originates in the central region of the cortex and propagates up and down the cortical depth toward the supragranular and infragranular layers (28). This finding is consistent with the hypothesis that changes in CBF start at the site of neural activity and propagate upstream toward the feeding arterioles and arteries (69). Curiously, the shorter CBF and BOLD HDR onset times in cortical layer IV is consistent with the expected order of neuronal current flow in the cortex (70), thus suggesting that the hemodynamic response could be preserving the temporal order of cortical neuronal events. While CBF cannot respond as fast to increased neuronal activity as electrical events, still the cerebral vasculature could be constructed to follow electrical activity as much as possible (12,16), making fMRI signals useful for probing cortical activity with short latencies, such as laminar communication.

4. Future Applications of DASL

The property of DASL to measure the three basic parameters related to quantification of CBF make the technique attractive for the measurement of hemodynamic parameters both in scientific studies of human brain function as well as in clinical studies of cerebrovascular diseases. The periodic repetition of the labeling function gives DASL superior advantage in achieving CBF measurements with high SNR due to the multiple sampling of the ASL data and due to the powerful noise reduction achieved by the fitting and filtering algorithms. Furthermore, DASL achieves unparalleled temporal resolution when compared to other ASL techniques, a fundamental feature to enable its application to the measurement of the hemodynamic response to functional brain stimulation and to the measurement of vascular transit times.

Recently, there has been renewed effort to map the perfusion territories of major cerebral arteries (71). While other ASL methods have been developed to measure arterial territories in the brain, none of the proposed techniques to date have enough temporal resolution to allow detailed characterization of the changes in vascular perfusion patterns associated with cerebrovascular diseases such as focal ischemia or hemorrhage. DASL is likely to be particularly suited for these applications where the changes in vascular territories are accompanied by changes in transit-times due to alteration in the perfusion patterns.

In conclusion, DASL is destined to constitute a versatile experimental platform for studying the spatial and temporal characteristics of functional cerebral hemodynamics. Further optimization of the technique will allow analysis of the vascular nature of the BOLD and the CBF responses, as well as the changes in vascular transit-times and perfusion territories associated with functional hyperemia.

Acknowledgments

References

1. Rakic P. Evolving concepts of cortical radial and areal specification. Prog Brain Res. 2002; 136:265–280. [PubMed: 12143387]

2. Ogawa S, Tank DW, Menon R, Ellermann JM, Kim SG, Merkle H, Ugurbil K. Intrinsic signal changes accompanying sensory stimulation: functional brain mapping with magnetic resonance imaging. Proc Natl Acad Sci U S A. 1992; 89:5951–5955. [PubMed: 1631079]

3. Phelps ME, Mazziotta JC, Huang SC. Study of cerebral function with positron computed tomography. J Cereb Blood Flow Metab. 1982; 2:113–162. [PubMed: 6210701]

4. Lieke EE, Frostig RD, Arieli A, Ts'o DY, Hildesheim R, Grinvald A. Optical imaging of cortical activity: real-time imaging using extrinsic dye-signals and high resolution imaging based on slow intrinsic-signals. Annu Rev Physiol. 1989; 51:543–559. [PubMed: 2653196]

5. Villringer A, Dirnagl U. Coupling of brain activity and cerebral blood flow: basis of functional neuroimaging. Cerebrovasc Brain Metab Rev. 1995; 7:240–276. [PubMed: 8519605]

6. Lauritzen M. Relationship of spikes, synaptic activity, and local changes of cerebral blood flow. J Cereb Blood Flow Metab. 2001; 21:1367–1383. [PubMed: 11740198]

7. Attwell D, Iadecola C. The neural basis of functional brain imaging signals. Trends Neurosci. 2002; 25:621–625. [PubMed: 12446129]

8. Iadecola C. Neurovascular regulation in the normal brain and in Alzheimer's disease. Nat Rev Neurosci. 2004; 5:347–360. [PubMed: 15100718]

9. Logothetis NK. The underpinnings of the BOLD functional magnetic resonance imaging signal. J Neurosci. 2003; 23:3963–3971. [PubMed: 12764080]

10. Lauritzen M. Reading vascular changes in brain imaging: is dendritic calcium the key? Nat Rev Neurosci. 2005; 6:77–85. [PubMed: 15611729]

11. Greenberg JH, Hand P, Sylvestro A, Reivich M. Localized metabolic-flow coupling during functional activity. Acta Neurol Scand. 1979; 60:12–13. [PubMed: 495039]

12. Cox SB, Woolsey TA, Rovainen CM. Localized dynamic changes in cortical blood flow with whisker stimulation corresponds to matched vascular and neuronal architecture of rat barrels. J Cereb Blood Flow Metab. 1993; 13:899–913. [PubMed: 8408316]

13. Woolsey TA, Rovainen CM, Cox SB, Henegar MH, Liang GE, Liu D, Moskalenko YE, Sui J, Wei L. Neuronal units linked to microvascular modules in cerebral cortex: response elements for imaging the brain. Cereb Cortex. 1996; 6:647–660. [PubMed: 8921201]

14. Gerrits RJ, Raczynski C, Greene AS, Stein EA. Regional cerebral blood flow responses to variable frequency whisker stimulation: an autoradiographic analysis. Brain Res. 2000; 864:205–212. [PubMed: 10802027]

15. Ehler E, Karlhuber G, Bauer HC, Draeger A. Heterogeneity of smooth muscle-associated proteins in mammalian brain microvasculature. Cell Tissue Res. 1995; 279:393–403. [PubMed: 7895277]

16. Harrison RV, Harel N, Panesar J, Mount RJ. Blood capillary distribution correlates with hemodynamic-based functional imaging in cerebral cortex. Cereb Cortex. 2002; 12:225–233. [PubMed: 11839597]

17. Patel U. Non-random distribution of blood vessels in the posterior region of the rat somatosensory cortex. Brain Res. 1983; 289:65–70. [PubMed: 6661656]

18. Masamoto K, Kurachi T, Takizawa N, Kobayashi H, Tanishita K. Successive depth variations in microvascular distribution of rat somatosensory cortex. Brain Res. 2004; 995:66–75. [PubMed: 14644472]

19. Duong TQ, Kim DS, Ugurbil K, Kim SG. Localized cerebral blood flow response at submillimeter columnar resolution. Proc Natl Acad Sci U S A. 2001; 98:10904–10909. [PubMed: 11526212]

20. Narayan SM, Santori EM, Toga AW. Mapping functional activity in rodent cortex using optical intrinsic signals. Cereb Cortex. 1994 Mar-Apr;4(2):195–204. [PubMed: 8038568]

21. Yang X, Hyder F, Shulman RG. Activation of single whisker barrel in rat brain localized by functional magnetic resonance imaging. Proc Natl Acad Sci U S A. 1996; 93:475–478. [PubMed: 8552664]

22. Yang X, Hyder F, Shulman RG. Functional MRI BOLD signal coincides with electrical activity in the rat whisker barrels. Magn Reson Med. 1997; 38:874–877. [PubMed: 9402186]

23. Kurth R, Villringer K, Curio G, Wolf KJ, Krause T, Repenthin J, Schwiemann J, Deuchert M, Villringer A. fMRI shows multiple somatotopic digit representations in human primary somatosensory cortex. Neuroreport. 2000; 11:1487–1491. [PubMed: 10841363]

24. Overduin SA, Servos P. Distributed digit somatotopy in primary somatosensory cortex. Neuroimage. 2004; 23:462–472. [PubMed: 15488396]

25. Kida I, Xu F, Shulman RG, Hyder F. Mapping at glomerular resolution: fMRI of rat olfactory bulb. Magn Reson Med. 2002; 48:570–576. [PubMed: 12210928]

26. Schafer JR, Kida I, Xu F, Rothman DL, Hyder F. Reproducibility of odor maps by fMRI in rodents. Neuroimage. 2006; 31:1238–1246. [PubMed: 16632382]

27. Silva AC, Lee SP, Iadecola C, Kim SG. Early temporal characteristics of cerebral blood flow and deoxyhemoglobin changes during somatosensory stimulation. J Cereb Blood Flow Metab. 2000; 20:201–206. [PubMed: 10616809]

28. Silva AC, Koretsky AP. Laminar specificity of functional MRI onset times during somatosensory stimulation in rat. Proc Natl Acad Sci U S A. 2002; 99:15182–15187. [PubMed: 12407177]

29. Lu H, Patel S, Luo F, Li SJ, Hillard CJ, Ward BD, Hyde JS. Spatial correlations of laminar BOLD and CBV responses to rat whisker stimulation with neuronal activity localized by Fos expression. Magn Reson Med. 2004; 52:1060–1068. [PubMed: 15508149]

30. Bonhoeffer T, Kim DS, Malonek D, Shoham D, Grinvald A. Optical imaging of the layout of functional domains in area 17 and across the area 17/18 border in cat visual cortex. Eur J Neurosci. 1995; 7:1973–1988. [PubMed: 8528473]

31. Malonek D, Grinvald A. Interactions between electrical activity and cortical microcirculation revealed by imaging spectroscopy: implications for functional brain mapping. Science. 1996; 272:551–554. [PubMed: 8614805]

32. Malonek D, Dirnagl U, Lindauer U, Yamada K, Kanno I, Grinvald A. Vascular imprints of neuronal activity: relationships between the dynamics of cortical blood flow, oxygenation, and volume changes following sensory stimulation. Proc Natl Acad Sci U S A. 1997; 94:14826–14831. [PubMed: 9405698]

33. Menon RS, Ogawa S, Strupp JP, Ugurbil K. Ocular dominance in human V1 demonstrated by functional magnetic resonance imaging. J Neurophysiol. 1997; 77:2780–2787. [PubMed: 9163392]

34. Kim DS, Duong TQ, Kim SG. High-resolution mapping of iso-orientation columns by fMRI. Nat Neurosci. 2000; 3:164–169. [PubMed: 10649572]

35. Cheng K, Waggoner RA, Tanaka K. Human ocular dominance columns as revealed by high-field functional magnetic resonance imaging. Neuron. 2001; 32:359–374. [PubMed: 11684004]

36. Goodyear BG, Menon RS. Brief visual stimulation allows mapping of ocular dominance in visual cortex using fMRI. Hum Brain Mapp. 2001; 14:210–217. [PubMed: 11668652]

37. Goodyear BG, Nicolle DA, Menon RS. High resolution fMRI of ocular dominance columns within the visual cortex of human amblyopes. Strabismus. 2002; 10:129–136. [PubMed: 12221492]

38. Kim SG, Duong TQ. Mapping cortical columnar structures using fMRI. Physiol Behav. 2002; 77:641–644. [PubMed: 12527012]

39. Fukuda M, Moon CH, Wang P, Kim SG. Mapping iso-orientation columns by contrast agent-enhanced functional magnetic resonance imaging: reproducibility, specificity, and evaluation by optical imaging of intrinsic signal. J Neurosci. 2006; 26:11821–11832. [PubMed: 17108155]

40. Sheth SA, Nemoto M, Guiou MW, Walker MA, Toga AW. Spatiotemporal evolution of functional hemodynamic changes and their relationship to neuronal activity. J Cereb Blood Flow Metab. 2005; 25:830–841. [PubMed: 15744249]

41. Narayan SM, Santori EM, Toga AW. Mapping functional activity in rodent cortex using optical intrinsic signals. Cereb Cortex. 1994 Mar-Apr;4(2):195–204. [PubMed: 8038568]

42. Narayan SM, Esfahani P, Blood AJ, Sikkens L, Toga AW. Functional increases in cerebral blood volume over somatosensory cortex. J Cereb Blood Flow Metab. 1995; 15:754–765. [PubMed: 7673370]

43. Berwick J, Martin C, Martindale J, Jones M, Johnston D, Zheng Y, Redgrave P, Mayhew J. Hemodynamic response in the unanesthetized rat: intrinsic optical imaging and spectroscopy of the barrel cortex. J Cereb Blood Flow Metab. 2002; 22:670–679. [PubMed: 12045665]

44. Martindale J, Mayhew J, Berwick J, Jones M, Martin C, Johnston D, Redgrave P, Zheng Y. The hemodynamic impulse response to a single neural event. J Cereb Blood Flow Metab. 2003; 23:546–555. [PubMed: 12771569]

45. Berwick J, Johnston D, Jones M, Martindale J, Redgrave P, McLoughlin N, Schiessl I, Mayhew JE. Neurovascular coupling investigated with two-dimensional optical imaging spectroscopy in rat whisker barrel cortex. Eur J Neurosci. 2005; 22:1655–1666. [PubMed: 16197506]

46. Narayan SM, Santori EM, Toga AW. Mapping functional activity in rodent cortex using optical intrinsic signals. Cereb Cortex. 1994 Mar-Apr;4(2):195–204. [PubMed: 8038568]

47. Friston KJ, Holmes AP, Poline JB, Grasby PJ, Williams SC, Frackowiak RS, Turner R. Analysis of fMRI time-series revisited. Neuroimage. 1995; 2:45–53. [PubMed: 9343589]

48. Boynton GM, Engel SA, Glover GH, Heeger DJ. Linear systems analysis of functional magnetic resonance imaging in human V1. J Neurosci. 1996; 16:4207–4221. [PubMed: 8753882]

49. Aguirre GK, Zarahn E, D'Esposito M. The variability of human, BOLD hemodynamic responses. Neuroimage. 1998; 8:360–369. [PubMed: 9811554]

50. de Zwart JA, Silva AC, van Gelderen P, Kellman P, Fukunaga M, Chu R, Koretsky AP, Frank JA, Duyn JH. Temporal dynamics of the BOLD fMRI impulse response. Neuroimage. 2005; 24:667–677. [PubMed: 15652302]

51. Detre JA, Zhang W, Roberts DA, Silva AC, Williams DS, Grandis DJ, Koretsky AP, Leigh JS. Tissue specific perfusion imaging using arterial spin labeling. NMR Biomed. 1994; 7:75–82. [PubMed: 8068529]

52. Calamante F, Thomas DL, Pell GS, Wiersma J, Turner R. Measuring cerebral blood flow using magnetic resonance imaging techniques. J Cereb Blood Flow Metab. 1999; 19:701–735. [PubMed: 10413026]

53. Barbier EL, Silva AC, Kim SG, Koretsky AP. Perfusion imaging using dynamic arterial spin labeling (DASL). Magn Reson Med. 2001; 45:1021–1029. [PubMed: 11378880]

54. Golay X, Hendrikse J, Lim TC. Perfusion imaging using arterial spin labeling. Top Magn Reson Imaging. 2004; 15:10–27. [PubMed: 15057170]

55. Kety SS. The theory and applications of inert gas exchange at the lungs and tissues. Pharmacol Rev. 1951; 3:1–41. [PubMed: 14833874]

56. Kety SS. Regional cerebral blood flow: estimation by means of nonmetabolized diffusible tracers --- an overview. Semin Nucl Med. 1985; 15:324–328. [PubMed: 3877343]

57. Barbier EL, Lamalle L, Decorps M. Methodology of brain perfusion imaging. J Magn Reson Imaging. 2001; 13:496–520. [PubMed: 11276094]

58. Detre JA, Leigh JS, Williams DS, Koretsky AP. Perfusion imaging. Magn Reson Med. 1992; 23:37–45. [PubMed: 1734182]

59. Williams DS, Detre JA, Leigh JS, Koretsky AP. Magnetic resonance imaging of perfusion using spin inversion of arterial water. Proc Natl Acad Sci U S A. 1992; 89:212–216. [PubMed: 1729691]

60. Edelman RR, Siewert B, Darby DG, Thangaraj V, Nobre AC, Mesulam MM, Warach S. Qualitative mapping of cerebral blood flow and functional localization with echo-planar MR imaging and signal targeting with alternating radio frequency. Radiology. 1994 Aug; 192(2):513–520. [PubMed: 8029425]

61. Kwong KK, Chesler DA, Weisskoff RM, Donahue KM, Davis TL, Ostergaard L, Campbell TA, Rosen BR. MR perfusion studies with T1-weighted echo planar imaging. Magn Reson Med. 1995; 34:878–887. [PubMed: 8598815]

62. Kim SG. Quantification of relative cerebral blood flow change by flow-sensitive alternating inversion recovery (FAIR) technique: application to functional mapping. Magn Reson Med. 1995; 34:293–301. [PubMed: 7500865]

63. Wong EC, Buxton RB, Frank LR. Implementation of quantitative perfusion imaging techniques for functional brain mapping using pulsed arterial spin labeling. NMR Biomed. 1997; 10:237–249. [PubMed: 9430354]

64. Wong EC, Buxton RB, Frank LR. A theoretical and experimental comparison of continuous and pulsed arterial spin labeling techniques for quantitative perfusion imaging. Magn Reson Med. 1998; 40:348–355. [PubMed: 9727936]

65. Barbier EL, Silva AC, Kim HJ, Williams DS, Koretsky AP. Perfusion analysis using dynamic arterial spin labeling (DASL). Magn Reson Med. 1999; 41:299–308. [PubMed: 10080277]

66. Zhang W, Williams DS, Detre JA, Koretsky AP. Measurement of brain perfusion by volume-localized NMR spectroscopy using inversion of arterial water spins: accounting for transit time and cross-relaxation. Magn Reson Med. 1992; 25:362–371. [PubMed: 1614321]

67. Silva AC, Kim SG. Pseudo-continuous arterial spin labeling technique for measuring CBF dynamics with high temporal resolution. Magn Reson Med. 1999; 42:425–429. [PubMed: 10467285]

68. Gao JH, Holland SK, Gore JC. Nuclear magnetic resonance signal from flowing nuclei in rapid imaging using gradient echoes. Med Phys. 1988; 15:809–814. [PubMed: 3237136]

69. Iadecola C. Regulation of the cerebral microcirculation during neural activity: is nitric oxide the missing link? Trends Neurosci. 1993; 16:206–214. [PubMed: 7688160]

70. Armstrong-James M, Fox K, Das-Gupta A. Flow of excitation within rat barrel cortex on striking a single vibrissa. J Neurophysiol. 1992; 68:1345–1358. [PubMed: 1432088]

71. Paiva FF, Tannus A, Silva AC. Measurement of cerebral perfusion territories using arterial spin labelling. NMR Biomed. 2007; 20:633–642. [PubMed: 17503440]
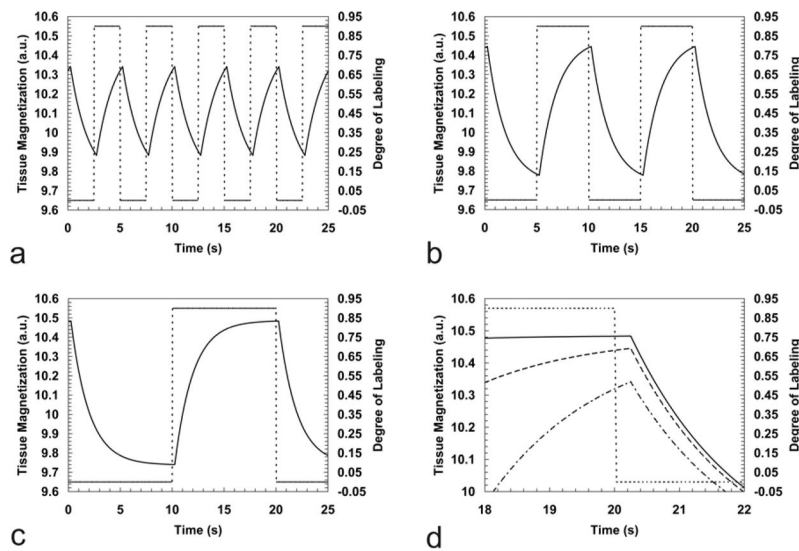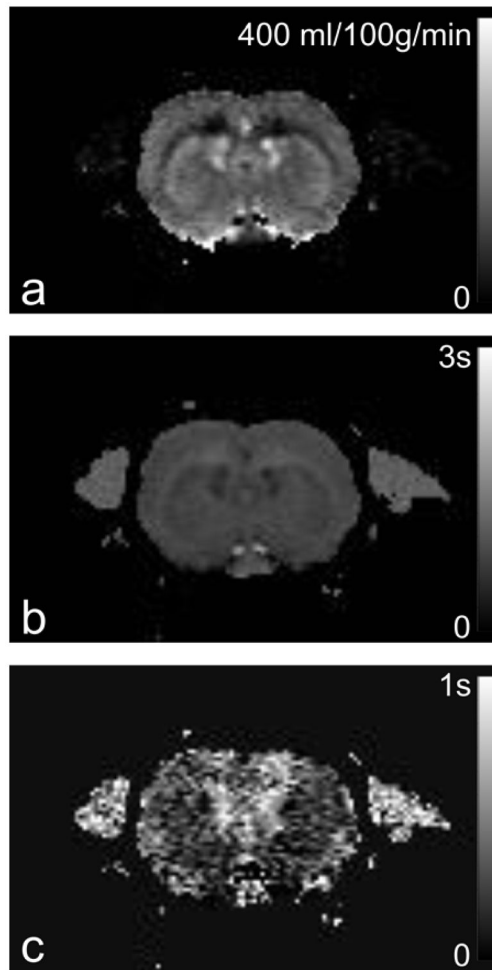
Figure 1.
Simulation of the tissue magnetization response to three different frequencies of the ASL function after steady state has been reached using the following parameters: T_{1app}=1.75 s, τ = 0.25 s, CBF = 150 ml / (100g · min) and α_0 = 0.90. Labeling frequencies of 0.20Hz (a), 0.10Hz (b) and 0.05Hz (c) are shown. The dashed lines show the labeling function (right-hand scales), and the dark lines show the corresponding tissue responses in arbitrary units (left-hand scales). An expanded scale plot of the maximum amplitude reached in each situation is shown in (d). Note that different labeling frequencies modulate the amplitudes of the tissue response, while the delayed tissue response is independently governed only by the transit time τ from the labeling plane to the detection region.
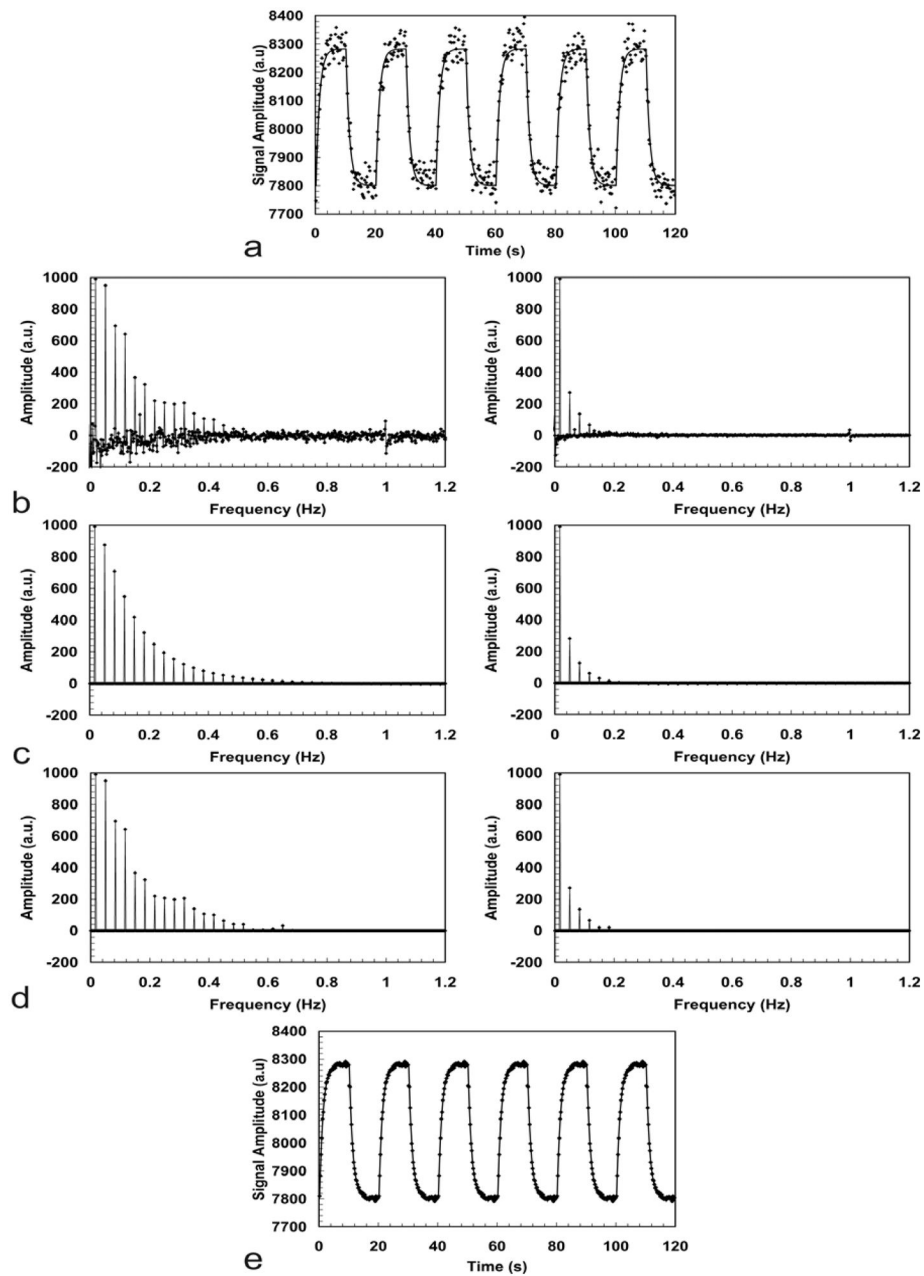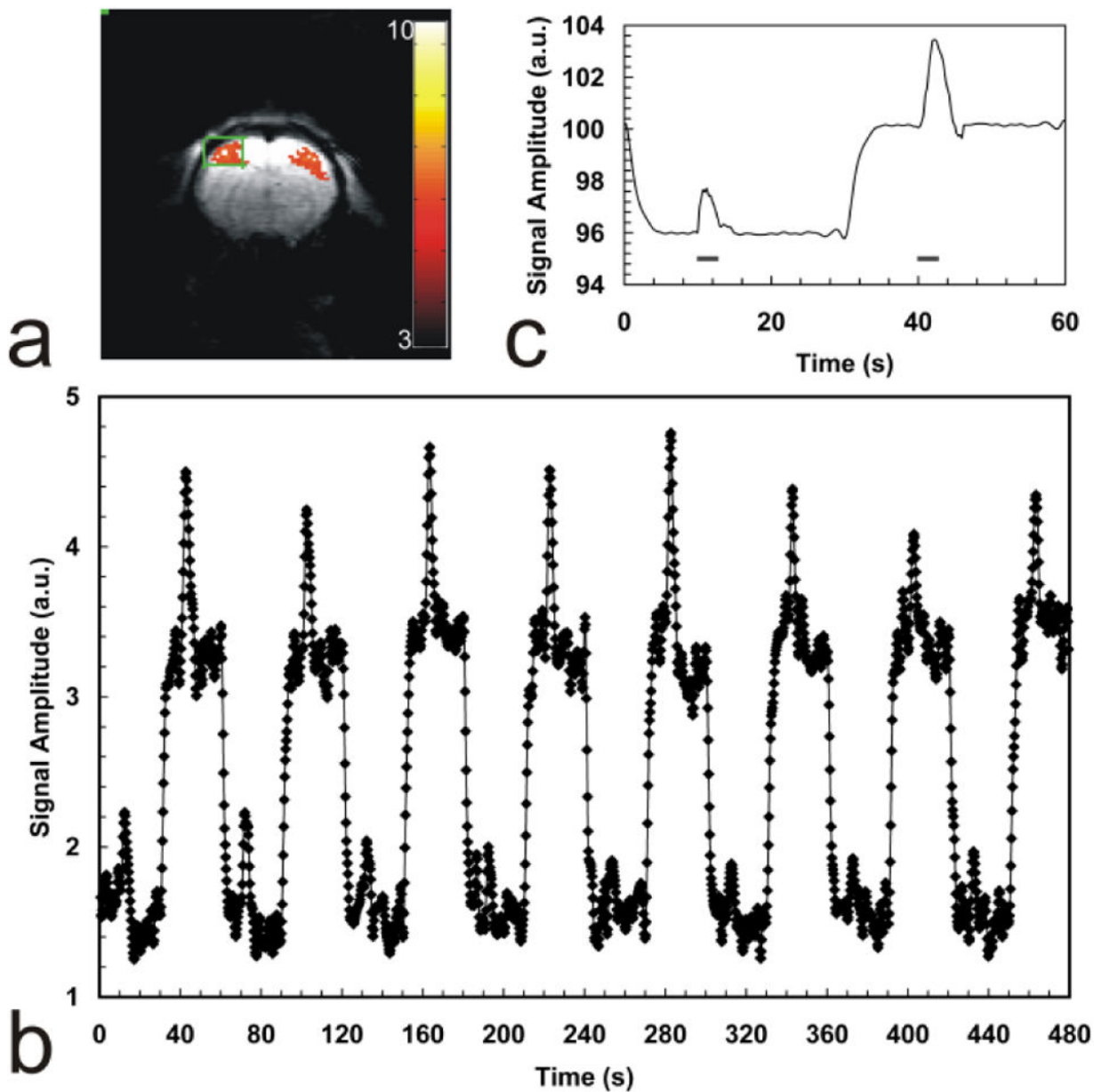
Figure 2.
Frequency filtering of DASL data obtained from an isoflurane-anesthetized rat at 7T using a labeling frequency of 0.05 Hz. (a) DASL time-course. (b) The real (left) and imaginary (right) components of the FT of the data. (c) The real (left) and the imaginary (right) components of the FT of the best fit to the model expressed by Eq. [10]. (d) The filtered data based only on the frequencies allowed by the model. In addition to removal of the noise, the peak around 1Hz due to the respiratory frequency is also filtered out. (e) The filtered DASL time-course.
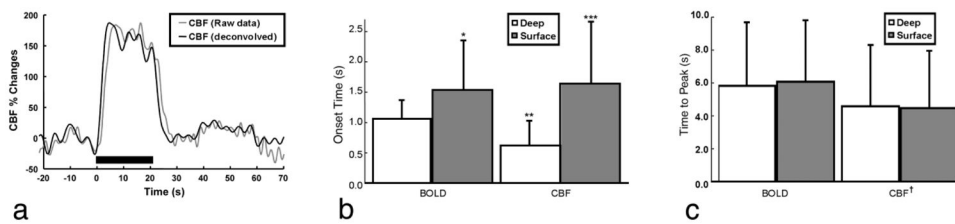
Figure 3.
Dynamic ASL parameter maps obtained from an isoflurane-anesthetized rat at 7T. A 2 mm-thick coronal slice that included the forelimb area of primary somatosensory cortex was imaged using a GE-EPI sequence with the following parameters: *TR/TE* = 250/20ms, *FOV* = 25.6 x 25.6 mm^2, matrix = 128 x 128, image acquisition time 49 ms. (a) CBF map obtained with high SNR and showing excellent anatomical definition of gray and white mater. (b) T_{1app} map. (c) Transit time map.

Figure 4.
Combined DASL-fMRI experiment. (a) t-score map of the BOLD functional response to bilateral stimulation of the rat forelimbs. Robust activation regions are present in both left and right primary somatosensory cortices. (b) Combined DASL-fMRI time-course. The functional hemodynamic is superimposed on top of the DASL experiment. (c) Data averaged into a single DASL cycle, obtained after fitting and filtering of the DASL curve. Stimulation periods are indicated by the horizontal bars underneath the hemodynamic response. The control phase of the DASL cycle displays a robust BOLD response, while the labeling phase shows the mixing of the functional BOLD and CBF contrast in anti-phase to each other.

Figure 5.
Temporal response of CBF and BOLD fMRI signals. **a:** Raw (gray) and deconvolved (black) CBF response curves obtained using ASL at 108 ms temporal resolution during electrical stimulation of the rat forepaw. The raw CBF curve was obtained at 9.4T and was deconvolved with the tissue T1 decay curve to produce the true CBF response. **b:** Averaged onset-times of CBF and GE-BOLD at 9.4T in the surface (gray bars) and deep (white bars) regions of the somatosensory cortex. (*) The onset of the BOLD response in the cortical surface was significantly later than deeper in the cortex (P < 0.03). (**) CBF changes in the deep cortex occurred earlier than the corresponding BOLD changes (P < 0.003). (***) The onset of superficial CBF changes was significantly delayed compared to deep in cortex (P < 0.004). **c:** Averaged time-to-peak of CBF and BOLD. There were no significant time-to-peak differences across regions within either BOLD (P > 0.28) or CBF (P > 0.39). (†) However, the CBF peak response occurred faster than the BOLD response in both regions (P < 0.001). Error bars = 1 std. dev. Adapted from ref. 27 with permission of Lippincott, William & Wilkins., and from ref. 67 with permission of Wiley-Liss Inc., Wiley Publishing Inc., a subsidiary of John Wiley & Sons.

Table 1

Onset Time and Time-to-Peak for CBF and BOLD Hemodynamic Responses to Somatosensory Stimulation in Rats

Contrast	CBF[*]		BOLD[*]		BOLD[§]	
Cortical Region	Deep	Surface	Deep	Surface	Layers I–III	Layers IV–V	Layer VI
Onset Time (s)	0.6 ± 0.4	1.6 ± 1.1	1.1 ± 0.2	1.5 ± 0.8	1.27 ± 0.43	0.59 ± 0.17	1.11 ± 0.45
Time-to-Peak (s)	4.4 ± 3.7	4.4 ± 3.5	5.8 ± 3.9	6.0 ± 3.8	4.37 ± 0.48	4.13 ± 0.62	4.79 ± 0.51

[*]Data from Ref. (27,67). Spatial resolution: 470 x 470 x 2000 μm^3. Temporal resolution 108 ms

[§]Data from Ref. (28). Spatial resolution: 200 x 200 x 2000 μm^3. Temporal resolution 40 ms